A compact magneto-optical trap apparatus for calcium

2009 Meas. Sci. Technol. 20 095303

(http://iopscience.iop.org/0957-0233/20/9/095303)

Meas. Sci. Technol. **20** (2009) 095303 (11pp) doi:10.1088/0957-0233/20/9/095303

A compact magneto-optical trap apparatus for calcium

U Dammalapati[1], I Norris[1], L Maguire[1], M Borkowski[2] and E Riis[1]

[1] SUPA, Department of Physics, University of Strathclyde, John Anderson Building, 107 Rottenrow East, Glasgow G4 0NG, UK
[2] Instytut Fizyki, Uniwersytet Mikołaja Kopernika, ul. Grudziądzka 5/7, 87-100 Toruń, Poland

E-mail: u.dammalapati@strath.ac.uk

Received 15 April 2009, in final form 1 June 2009
Published 14 July 2009
Online at stacks.iop.org/MST/20/095303

Abstract
We present a compact apparatus for laser cooling and trapping of atomic calcium. The set-up consisting of a Zeeman-slowed thermal beam and a magneto-optical trap (MOT) has potential use for studying optical lattices, optical clocks, sensitive trace analysis, ultra-cold collisions and the feasibility of achieving quantum degeneracy in an alkaline earth element. Construction of the apparatus is described as well as the characterization of the trap in terms of atom number and lifetime. The lifetime results are compared with a rate equation model for the system.

Keywords: calcium, Zeeman slower, laser cooling, magneto-optical trap, lifetime

(Some figures in this article are in colour only in the electronic version)

1. Introduction

The first demonstration of magneto-optical confinement of neutral atoms was one of the path-breaking experiments in atomic physics [1]. This technique is now used as a workhorse in a wide range of experiments with different physics motivations. In particular, the operation of a magneto-optical trap (MOT) has been extended for use with elements outside the alkali metal group. The MOT is the starting point for further exploitation of laser cooling and trapping methods. Along with evaporative cooling of atoms it has, e.g., resulted in the experimental realization of Bose–Einstein condensation (BEC) [2, 3]. This has opened the new field of coherent matter wave physics and established an interesting interface between atomic and condensed matter physics. Beyond this, the MOT provides a source of laser cooled and trapped atoms in several rapidly expanding fields of atomic physics including optical frequency standards, precision measurements, cold collision studies and atom interferometry. An extensive literature survey on laser cooling and trapping techniques can be found in the review [4].

The flurry of activity in ultra-cold atomic physics brought about by laser cooling is mainly limited to the stable alkali atoms. This is primarily due to their convenient atomic structure, availability of laser sources and ease of handling. Notable exceptions to this have been the realization of BEC in helium [5, 6] and ytterbium [7] and the work on optical atomic clocks in calcium [8] and strontium [9].

The two-electron systems of the alkaline earth elements (and ytterbium) offer a rich and multipurpose internal level structure. They all have several stable isotopes with both bosons (nuclear spin zero) and fermions. In these elements, the $ns^2\ {}^1S_0$–$nsnp\ {}^1P_1$ dipole transition is convenient for laser cooling and trapping in the ground state. The transitions are strong and are ideal for both beam slowing and magneto-optic trapping. For the bosonic isotopes, which generally are the most abundant, the lack of a nuclear spin means that the temperatures obtained are limited to the Doppler temperature of around 1 mK. However, the intercombination line $ns^2\ {}^1S_0$–$nsnp\ {}^3P_1$ can be used for a second stage of laser cooling and/or as an optical frequency standard because of its narrow linewidth.

The bosonic isotopes have been used for, e.g., the development of optical clocks [8], cold collision studies [10] and atom interferometry [11]. The observation of quantum degeneracy has not been realized so far in an alkaline earth element. Among these, a highest phase-space density of 0.1 was reported for Sr [12]. However, BEC has been realized in ytterbium [7] whose atomic structure is similar to that of the alkaline earth atoms. Isotopes with nuclear spin possess

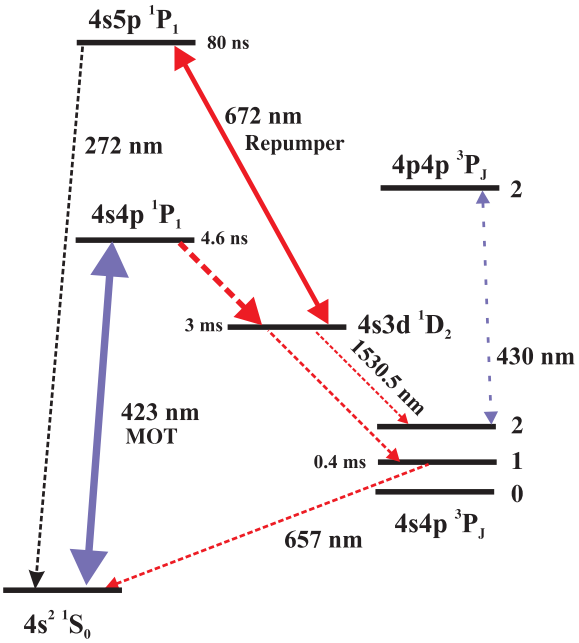

Figure 1. Energy level diagram of the calcium atom with vacuum wavelengths and lifetimes indicated for the transitions of relevance. The main cooling transition is the $^1S_0$–$^1P_1$ transition at 423 nm. Atoms are lost from this cooling cycle by a weak decay to the $^1D_2$ state. The decay to the metastable $^3P_2$ state represents the main loss out of the system while repumping is possible on the 672 nm transition.

hyperfine structure in the excited state as well as magnetic substructure in the ground state. Consequently sub-Doppler cooling is possible and has indeed been reported for ^{87}Sr [13]. This is also one of the candidates for future optical frequency standards and for quantum information processing [14]. The apparently highly forbidden $^1S_0$–$^3P_0$ transition in ^{87}Sr can actually be driven by a laser due to hyperfine interactions between the $^3P_1$ and $^1P_1$ states [15].

Calcium, another alkaline earth element, is also a candidate for the above experiments as well as atom trap trace analysis of Ca isotopes [16]. The intercombination 4s^2 $^1S_0$–4s4p $^3P_1$ transition at 657 nm has a linewidth of 400 Hz and has been proposed as a future optical frequency standard [8]. Natural calcium has six isotopes with atomic mass units and abundances 40 (96.941%), 42 (0.647%), 43 (0.135%), 44 (2.086%), 46 (0.004%) and 48 (0.187%), respectively. The ground-state nuclear spin of the even isotopes is zero and for the odd isotopes it is 7/2 [17]. The 4s^2 $^1S_0$–4s4p $^1P_1$ dipole transition at 423 nm (figure 1) is suitable for laser cooling and trapping to the Doppler limit. The $^1P_1$ level has a lifetime of 4.6 ns corresponding to a natural linewidth $\Gamma = 2\pi \times 35$ MHz. The saturation intensity (I_s) on resonance for this transition is 60 mW cm^{-2} and the Doppler limit is about 1 mK.

Although the 4s^2 $^1S_0$–4s4p $^1P_1$ transition is not a closed system, laser cooling is possible without repumping. This is due to the fact that the branching ratio to the $^1D_2$ level is only about 1:100 000 [18]. While this is sufficient for slowing a beam, it does limit the observed lifetime of the MOT. For typical experimental parameters for the MOT volume and temperature, the majority of the $^1D_2$ atoms will decay to the ^3P levels (with a lifetime of 1.5(4) ms [19]) before they leave the trapping volume. The atoms decaying to the $^3P_1$ state return to the ground state with a lifetime of 0.4 ms and rejoin the cooling cycle while the $^3P_2$ state is metastable. It therefore represents the main leak out of the system.

The lifetime of the MOT can be extended and the atom number can be increased by intercepting this decay while the atoms are in the $^1D_2$ state. Semiconductor laser diodes with sufficient power are available to drive the 672 nm 4s3d $^1D_2$–4s5p $^1P_1$ transition, the upper level of which can decay to the ground state [8].

Atoms that are lost to the $^3P_2$ level can be brought back to the $^1S_0$ ground state by two repumping methods. The Hamburg group [20] has demonstrated optical pumping via the higher 4p4p $^3P_2$ level to the 4s4p $^3P_1$ state with a subsequent decay to the ground state. We have demonstrated repumping of the metastable atoms back to the 4s3d $^1D_2$ state using a laser at 1530.5 nm [21]. From here they get another chance of decaying to the ground state via the 4s4p $^3P_1$ state or getting repumped on the 672 nm transition. In addition, the Hamburg group made use of the metastable $^3P_2$ state atoms for second stage cooling with the narrow $^3P_2$–$^3D_3$ transition at 2 μm achieving sub-Doppler temperatures for calcium [22].

This paper describes and reports on the operation of a compact apparatus for realizing a calcium magneto-optic trap. It consists of a laser system where the 423 nm light for the $^1S_0$–$^1P_1$ cooling transition is generated by frequency doubling of a Ti:sapphire laser, an atomic oven, which emits a collimated thermal beam, a Zeeman slower and a conventional MOT formed by three orthogonal, retro-reflected beams.

This paper is organized as follows. Section 2 describes the various components of the experimental set-up. In section 3, we describe the results, characterization and optimization of the MOT. The influence of various parameters such as the lifetime of the $^1D_2$ state, trap beam size, velocity of the trapped atoms, loss channels on the MOT lifetime and atom number calculated by a rate equation model is given. In section 4, we summarize with future improvements that can be made to the set-up.

2. Experimental set-up

The experimental apparatus can be divided into several sections: (2.1) laser sources and optics, (2.2) the calcium oven for the production of a collimated atomic beam, (2.3) the Zeeman slower to produce a higher flux of slow atoms from the thermal distribution from the oven, (2.4) a deflection and two-dimensional optical molasses stage for delivering the slowed atoms to the magneto-optical trap, (2.5) the MOT stage and (2.6) the detection system. The layout of the optical set-up is shown in figure 2, while the parts related to the vacuum system (2.2–5) are shown schematically in figure 3. The apparatus is maintained at an ultra-high vacuum with a turbo-molecular pump at the oven end, and an ion pump is directly attached to the MOT chamber. A pneumatic gate valve separates the two sections enabling easy servicing of both parts.

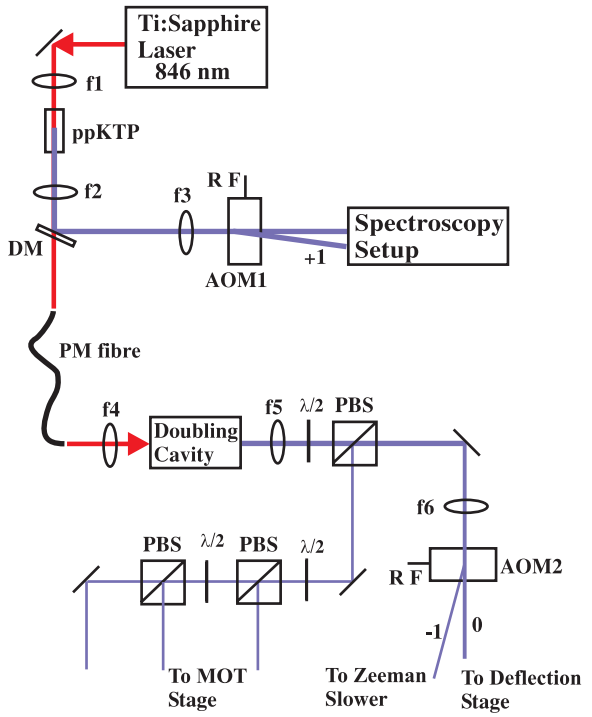

Figure 2. Optical layout of the calcium laser cooling and trapping experiment. ppKTP, frequency doubling crystal; DM, dichroic mirror; f1-6, lenses; AOM1 (RF = 80 MHz) and AOM2 (RF = 202 MHz), acousto-optic modulators; PM fibre, polarization maintaining, single-mode fibre; PBS, polarizing beam splitter; $\lambda/2$, half-wave plate.

2.1. Laser sources and 423 nm light generation

The 423 nm laser light required for the experiment is generated in three stages. An 8 W diode pumped solid-state laser at 532 nm (Coherent Verdi-V8) is used as a pump laser for producing 700–800 mW of 846 nm light from a Microlase MBR-110E, single frequency CW, Ti:sapphire laser. We use two periodically poled $KTiOPO_4$ (ppKTP), quasi-phase matching, nonlinear crystals for the generation of 423 nm light. One is used in a single-pass geometry for frequency stabilization of the Ti:sapphire laser using saturated absorption spectroscopy in a hollow-cathode lamp, while the other is placed in a resonant enhancement cavity generating the light used for the laser cooling and trapping experiment. The characterization of these crystals for efficient production of 423 nm light, the enhancement cavity design and operation have been described elsewhere [23]. The stabilization scheme enabling the second harmonic light to be locked about half the linewidth to the red of the calcium $^1S_0$–$^1P_1$ resonance transition has also been described elsewhere [24].

Around 100 mW of the 423 nm light is required for various stages of the laser cooling and trapping experiment. For this, the 846 nm light is coupled through a polarization maintaining (PM) single-mode fibre and transported to the optics table where the doubling cavity and the MOT apparatus are situated. For an input power of 400–500 mW, the overall efficiency of this custom-made doubling cavity is 20–25%. At this level of efficiency, which is less than the optimum one reported in [25], we achieve stable and reliable long-term locking. The blue light is distributed to the MOT laser beams, the Zeeman slower and the deflection stage. The light for the MOT beams is expanded to a $(1/e^2)$ beam diameter of 13 mm. It is then split into three beams of equal power (10 mW). The light for the Zeeman slower is obtained as the first-order down-shifted beam from an acousto-optic modulator operating at 202 MHz. Around 20–25 mW of power is available in this order. The zeroth order from this AOM is expanded to a 14 mm diameter beam and used for the deflection stage.

2.2. The oven

The oven is designed to satisfy two main requirements. As the vapour pressure of calcium is low compared with, e.g., alkali metals, the temperature needed for obtaining a sufficient flux of atoms is of order 500 °C. Hence, the oven and surroundings have to be constructed to produce and withstand this temperature as well as dissipate the associated power. The second consideration is that it is desirable for the oven to produce a well-collimated beam of calcium atoms [25]. The schematic of the oven is shown in figure 4. It is made of two 15 mm long stainless steel cylindrical capsules (1) with an inner diameter of 17 mm. They are held together with two, 34 mm outer diameter, flanges similar to DN16 conflat

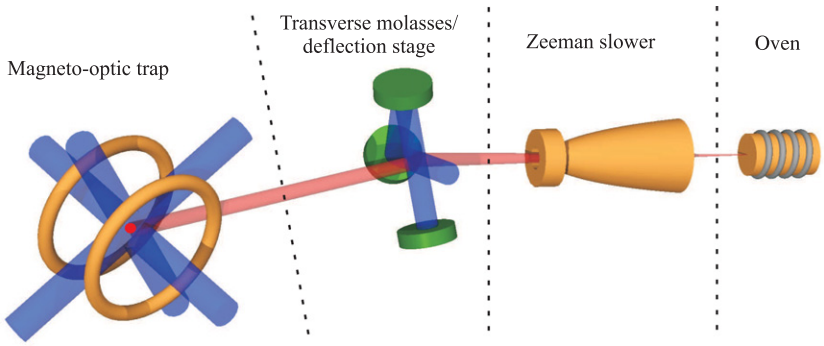

Figure 3. Various stages of the calcium laser cooling and trapping experiment. Shown are the atomic beam (red), the Ca oven (orange) and the heater coil (grey), the deflection stage mirrors (green), the deflection laser beam (blue) and the MOT stage with MOT coils (orange) and MOT beams (blue). Details of each stage are given in the text.

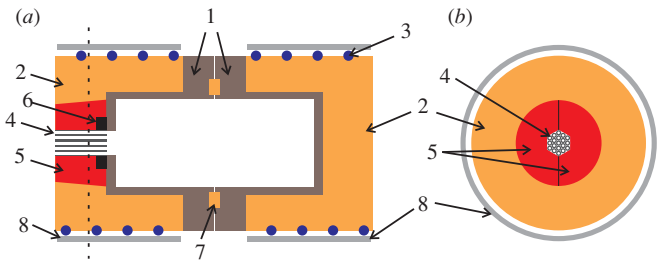

Figure 4. Cross-sections of the Ca oven. A stainless steel capsule (1) contains the Ca metal and is surrounded by a copper shell (2) heated by coaxial heaters (3). Nineteen stainless steel capillaries (4) collimate the beam. The capillaries have a 0.5 mm inner diameter, are 10 mm long and are held in place by two copper pieces (5) forming a hexagonal hole in the middle and a conical outer surface. Once assembled this unit is pressed into a matching cone formed in one of the copper shells. A stainless steel disk (6) with a hexagonal hole in the middle restricts the access of the hot calcium to the surrounding copper. Similarly, the design of the stainless steel capsules restricts the access of the calcium to the copper gasket (7), which seals the oven. Two stainless steel tubes (8) hold the heaters tightly against the copper shells and provide some insulation of the oven. (*a*) Longitudinal cross-section. A transverse cross-section through the oven at the dashed line is shown in (*b*).

flanges except that no knife-edge has been incorporated and the seal is therefore formed by an uncompressed copper gasket (7). The outer diameter of the steel capsules has a slight taper (1°) to form a tight mechanical and thermal contact with two outer copper cylinders (2) with an identical inner taper. The outer diameter of the copper cylinders is 34 mm. The outer surface is provided with semicircular grooves into which coaxial (Thermocoax) heater wires (3) are wound forming a good thermal contact. The heaters are held in place firmly by two cylindrical stainless steel shells (8) with minimal thermal contact with the heaters. The oven is filled with granules of high purity natural calcium.

In order to obtain a well collimated beam of calcium atoms, the copper cylinder forming the front end of the oven contains 19 stainless steel capillary tubes (inner diameter (ID) 0.5 mm, outer diameter (OD) 0.8 mm and length 10 mm (4)), which are held tightly to form a hexagon (5) with two copper pieces. The front and rear parts of the oven are heated independently, and the temperatures of both ends are measured with K-type thermocouples. In order to avoid clogging of calcium in the capillaries, the front end of the oven is operated at a higher temperature than the back end by about 20–30 °C. The typical operating temperature of the oven is 450–490 °C. The beam emerging from the oven is approximately 4 mm in diameter with a full-angle divergence of less than 6°. However, as far as the experiment is concerned the collimation is limited to approximately 2° by the slowing laser beam size.

The whole oven is mounted on a DN75 conflat flange with three posts of low thermal conductivity. This flange provides electrical feedthroughs for the heater wires and thermocouples as well as heat sinking for the end connectors of the Thermocoax, which is designed for room-temperature operation. The oven is surrounded by a 50 mm diameter water cooled copper tube in order to minimize direct heating of the vacuum chamber.

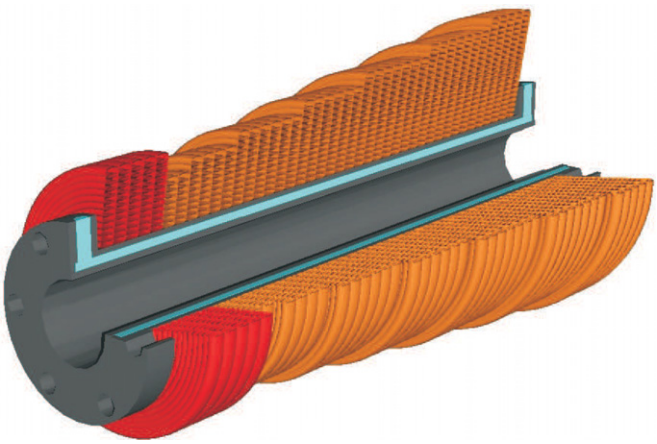

Figure 5. A cross-section of the Zeeman slower. The overall length of the Zeeman slower is 140 mm. The tapered main coil is shown in orange while the separate end coil at the exit is shown in red. The maximum coil diameter at the entrance of the slower is 60 mm. The coils are wound on a double-walled vacuum pipe with an outer diameter of 20 mm. This allows cooling water (blue) to carry away heat from the centre.

2.3. The Zeeman slower

The first step in laser cooling of atoms emerging from a thermal atomic beam is to bring the longitudinal velocity down from typically a few hundred m s^{-1} to a few tens of m s^{-1}. A widely used method is Zeeman tuned slowing [27], where atoms pass through a spatially varying magnetic field designed to keep the atomic transition resonant with a counter-propagating laser by compensating the decelerating atoms' changing Doppler shift with an equal but opposite Zeeman shift. This scheme is not generally applicable when the cooling transition is not closed [28], but as mentioned in section 1 the leak out of the cooling cycle without a repumper (for calcium) is 1:100 000 whereas less than 25 000 photons are required to bring the most probable velocity from the oven to rest.

In a well-designed Zeeman slower, all atoms up to a certain maximum initial velocity are slowed to a few tens of m s^{-1}. This corresponds to a massive increase of the low-velocity flux compared with the initial Maxwell–Boltzmann distribution from the oven. In order to increase the beam flux, it is obviously desirable to have this maximum initial velocity as high as possible, but the requirements for the maximum magnetic field and the length of the slower increase with this velocity approximately linearly and quadratically, respectively. Furthermore, transverse heating due to photons spontaneously emitted away from the beam axis results in a progressively larger expansion of the cooled beam with a longer slower. As a suitable compromise, we have designed a relatively short Zeeman slower for our calcium experiment capable of slowing atoms from about 500 m s^{-1} down to a mean velocity of ∼60 m s^{-1}. At an oven temperature of 490 °C, this corresponds to 19% of the beam flux. A right circularly polarized laser light is used as a slowing laser beam.

Figure 5 shows the design of the Zeeman slower coil. It is 140 mm long and has a decreasing magnetic field made up from two independent coils. A tapered solenoid is designed to follow the decreasing Doppler shift of the slowed atoms while

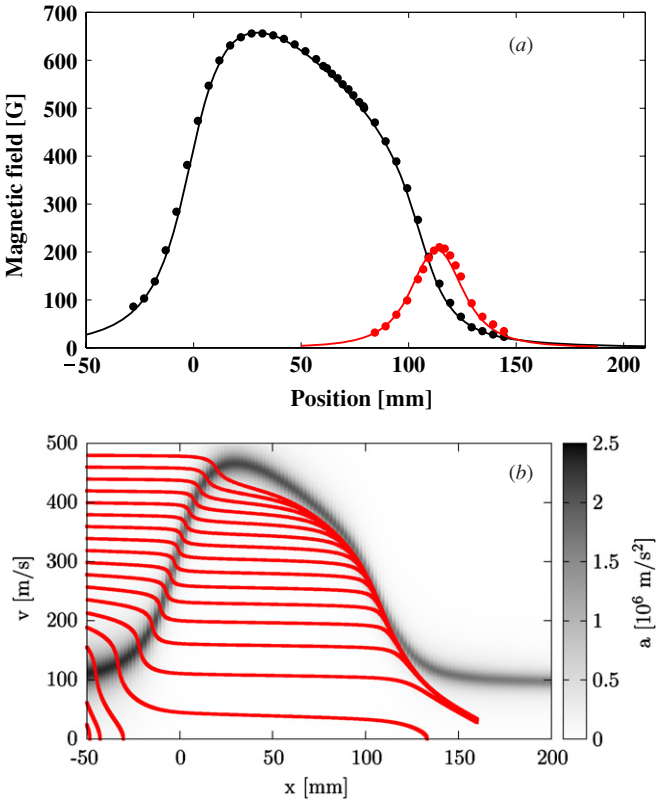

Figure 6. (*a*) The variation of the magnetic field with distance. Black: main coil. Red: end coil. The points show the measured values at 10 A (main coil) and 9.9 A (end coil), while the full curves are calculated based on the coil design. (*b*) Atomic phase-space trajectories in the Zeeman slower are shown in red for a range of initial velocities. The spatially and velocity dependent acceleration as given by equation (1) is shown by the grey scale on the right.

a fixed width coil at the exit provides an additional flexibility to tailor the magnetic field near the end. The coil is wound from rectangular copper wire of cross-section 2.8 mm × 1 mm. It is designed to run at up to 10 A in each coil consuming about 40 W of power. The rectangular wire was chosen to provide closer packing and hence better thermal conductivity throughout the coil. Cooling is provided in two ways. The central vacuum pipe is double walled allowing a thin layer of water to flow immediately below the inner surface of the coil. Cold water also flows through a soft plastic pipe wrapped around the outer surface of the coil.

The number of turns on each layer of the coil was chosen to approximate the ideal spatial variation of the field [27]. The magnetic field on the symmetry axis is calculated by adding up the contributions from all the individual turns. As shown in figure 6(*a*), this provides good agreement with the values measured with a Hall probe. For the volume of interest for the Zeeman slower, we can assume that the field is independent of the radial position.

The motion of the atoms through the Zeeman slower is modelled using a one-dimensional Newtonian model. The initial velocity distribution is given by the Maxwell–Boltzmann distribution. The dynamics of the slowing process is then obtained by integrating the expression for the light pressure force [4],

$$m\ddot{x} = \hbar k \frac{\Gamma}{2} \frac{I/I_s}{1 + I/I_s + (2\Delta(x, v)/\Gamma)^2}, \tag{1}$$

where the position (x) and velocity (v) dependent detuning is

$$\Delta(x, z) = \Delta_{\text{las}} - kv + \mu B(x) \tag{2}$$

and Δ_{las} is the laser detuning at zero magnetic field ($-2\pi \times$ 225 MHz), $\hbar$ is Planck's constant divided by 2π, Γ is the linewidth of the transition, k is the wave number, I_s is the saturation intensity of the transition, $\mu = 2\pi \times 1.4$ MHz G^{-1} is the magnetic moment and the mass, m, is 40 atomic mass units. Included in our model is the spatial variation of the intensity, I, along the beam axis. This is due to the slowing beam used in the experiment being focused on a radius of 2.1 mm at the oven exit. The transverse intensity variation of the slowing beam is accounted for by including trajectories with reduced intensities corresponding to atoms across the spatial atomic distribution experiencing the Gaussian laser profile.

Modelling of the atomic trajectories in the Zeeman slower has been used to guide the design and to estimate the optimum operating conditions. For a parameter set similar to what is used in the experiment the deceleration given by (1) is shown in figure 6(*b*) as a function of position and atomic velocity. Also shown here are a number of phase space trajectories for different initial velocities. For the small fraction of atoms with an initial velocity of less than 200 m s^{-1} the deceleration experienced as they enter the magnetic field of the slower is sufficient that they are eventually brought to a halt and lost out of the beam. Atoms with initial velocities between 200 and 500 m s^{-1} experience only a slight deceleration as they enter the slower. They then travel largely unaffected till they hit the ridge of maximum deceleration, travel along this ridge and are finally brought to a velocity in the region of 60 m s^{-1} at the exit of the slower.

Investigations of the numerical model with lower laser intensities reveal that atoms are lost from the slower at velocities of around 200 m s^{-1}, which is greater than the MOT capture velocity. This is a result of the scattering rate being insufficient for the changing Doppler shift to keep up with the rapidly spatially varying Zeeman shift near the exit of the coil. For the laser beam size used in the experiment trajectories experiencing an intensity of less than that on the beam axis will always be encountered and effects of that can be expected. In contrast, heating due to radial spontaneous emission (less than 3 m s^{-1}) is negligible compared with the initial transverse velocity distribution.

2.4. The deflection stage

The deflection section is a two-dimensional, transverse molasses stage. It serves the dual purpose of transversely cooling the slowed atoms and deflecting them away from the remaining hot atoms in the Boltzmann distribution from the oven. A single laser beam of diameter 14 mm and a power of up to 20 mW is retro-reflected in a figure-of-four geometry formed by two mirrors placed at an angle of incidence of

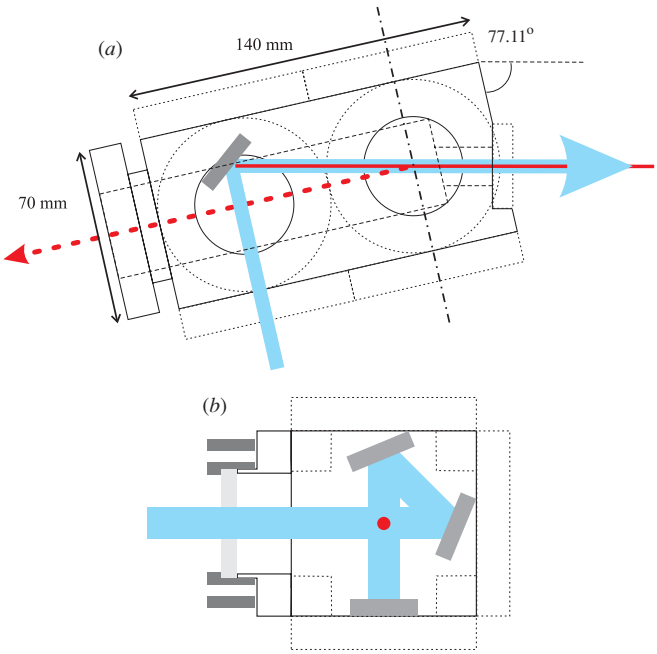

Figure 7. Schematic diagram of the deflection stage, which is mounted directly on the end of the Zeeman slower. (*a*) Longitudinal section. The atomic beam enters from the right and is overlapped with the slowing beam, which enters from the bottom and is reflected off a mirror inside the vacuum. The transverse molasses deflects slowed atoms along the dotted line. It is not shown in this view but implemented in a plane along the dash-dotted line. (*b*) shows the cross-section along this line and the figure-of-four path, the light follows to provide the two orthogonal standing waves for the transverse cooling. For clarity, the vacuum flanges and windows are only indicated with faint dashed lines apart from the window in (*b*) showing the lead-seal vacuum viewport design [30].

22.5° and a single retro-mirror all mounted within the vacuum chamber. This configuration minimizes the power loss, which is essential in order to reduce the transverse velocity of the resulting beam in this purely Doppler cooled system. A further advantage of this stage is the isotope selective deflection of calcium atoms to the MOT chamber. This method has been successfully employed for atom trap trace analysis of calcium isotopes [16].

The estimated velocity damping time constant in this molasses stage is 25 μs [4] for a laser power of 10 mW and a detuning of half the linewidth below resonance. Thus, even the fastest atoms of interest (100 m s^{-1}) spend several damping times in this section and will leave in a direction orthogonal to the cooling beams and with an expected transverse temperature comparable to the Doppler temperature. This results in a deflection of the slowed atoms by an angle of 12.9° in the vertical plane and into the direction of the MOT chamber.

The vacuum chamber shown in figure 7 consists of a rectangular stainless steel block of dimension 70 mm × 70 mm × 150 mm with 10 conflat ports. The end ports provide entrance and exit for the atoms while slowing and transverse molasses laser beams enter through anti-reflection (AR) coated windows. In order to ensure that a window is not in the direct line of sight of the atomic beam, the slowing beam is directed by a silver coated mirror mounted inside the vacuum at an angle of incidence of about 40°.

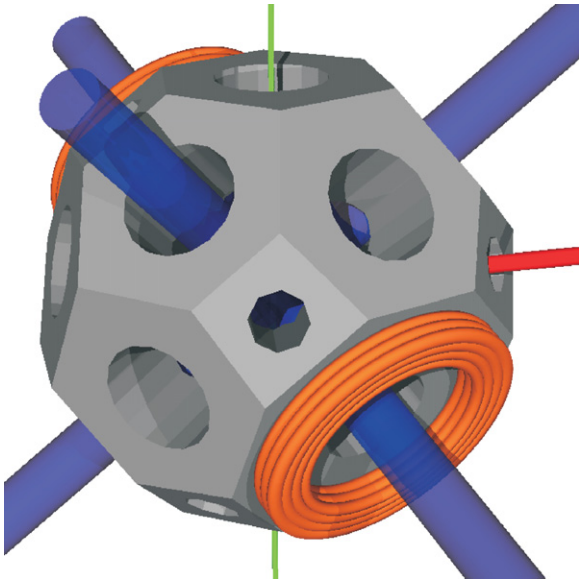

Figure 8. A three-dimensional view of the calcium MOT chamber without the vacuum windows. The (blue) MOT laser beams intersect in the centre and the chamber is oriented such that the green line shown is oriented vertically. The slowed atoms (red) enter from the right. Magnetic coils are shown in orange. Larger holes shown in figure correspond to DN40 and smaller ones to DN25.

2.5. The MOT chamber

The experimental chamber for magneto-optical trapping of calcium atoms is custom made from a single block of 316LN stainless steel. The final shape shown in figure 8 resembles a sphere but with 22 flat surfaces all of which have conflat flange ports machined into them. The basic structure of the chamber is a square cuboid providing the three orthogonal axes for the MOT. A 40 mm hole is drilled through the metal in each of these directions, and a DN40 conflat flange is formed on the surface. Near each of the diagonals a 40 mm hole is drilled through the centre and a DN40 conflat flange formed on a surface created normal to this direction. Additional eight surfaces are created on the resulting polyhedron and connected through the centre with 25 mm holes. DN25 conflat flanges are formed on these surfaces. This geometry is chosen to enable the co-location of a MOT and a four-beam optical lattice [29]. In the present set-up, one of the lattice directions is oriented vertically and the atoms are brought in from the deflection stage through one of the DN25 ports. The MOT chamber is situated at a distance of 313 mm from the deflection stage. The viewports on the MOT chamber as well as those of the deflection chamber are of a home-made design, which has been described previously [30], incorporating high-quality AR coated windows with a large area of optical access. Low loss windows minimizing the intensity imbalance in the MOT region are essential for a Doppler cooled system.

The magnetic field gradient required for the MOT in the present set-up is obtained by two anti-Helmholtz coils placed outside the chamber and each consisting of 12 turns of water cooled, square profile copper pipe. The inner coil diameter is 70 mm and they are separated by 132 mm. The operating

current of the coils is 210 A. This results in a magnetic field gradient of 32 G cm^{-1} on the symmetry axis.

The capture velocity of atoms in a trap depends on the trap laser intensity, detuning, beam size and the characteristics of the magnetic field. A one-dimensional Newtonian model, similar to that used for modelling the Zeeman slower, shows that the capture velocity is relatively independent of the magnetic field gradient for values achievable with our coil set-up. The process of capturing an atom into the MOT essentially works by first bringing the atom to a halt as it travels across the optical molasses and before escaping on the other side. Once stopped, the atom then falls into the MOT as explained by the familiar magneto-optic trapping mechanism. By modelling the spatially and velocity dependent acceleration in a similar way to the Zeeman slower, we estimate the capture velocity of the MOT to be 70 m s^{-1}.

2.6. The detection system

To detect the fluorescence of the Ca MOT a low noise transimpedance photodiode amplifier is used (Femto PD Model: LCA-S-400K-SI). The conversion gain of the photodiode at 423 nm is 1.0×10^6 V/W. The fluorescence from the MOT is imaged with an achromatic lens system with an effective focal length $f = 36$ mm positioned at a distance of 86 mm from the centre of the chamber. The corresponding solid angle is 0.15. To minimize the scattered light, inside walls of the MOT chamber are coated with carbon paint.

3. Results and discussion

As a first step, the longitudinal velocity distribution from the oven was measured. Fluorescence from the beam was recorded as the frequency of a 10 mW counter-propagating collinear laser beam was scanned across the distribution (figure 9(*a*)). The spectrum was compared with the expected signal from a Maxwell–Boltzmann distribution from an effusive oven operating at 456 °C as measured with a thermocouple. The zero-velocity calibration was confirmed with a Doppler-free spectrum measured by exciting the atoms perpendicularly to the atomic beam.

The velocity distribution of the atoms reaching the MOT chamber was measured using a time-of-flight (TOF) method. The laser beams of the deflection stage were gated on for 1 ms allowing a pulse of atoms to be deflected and travel to the MOT chamber. Fluorescence from these atoms is observed using a resonant laser beam propagating perpendicularly to the atomic direction. The TOF signal is converted back to fluorescence as a function of velocity and is shown in figure 9(*b*). These data are fitted with the expected curve for a Gaussian velocity distribution centred at 72 m s^{-1} and with a width of 26 m s^{-1}. Due to the atoms being gated on for a finite time (1 ms), this method overestimates the width of the distribution by a few m s^{-1}.

The experimental set-up has been characterized by various parameters for achieving optimal performance. In figure 10(*a*), the relative number of trapped atoms is shown as a function of power in the deflection stage. We observe that the optimum

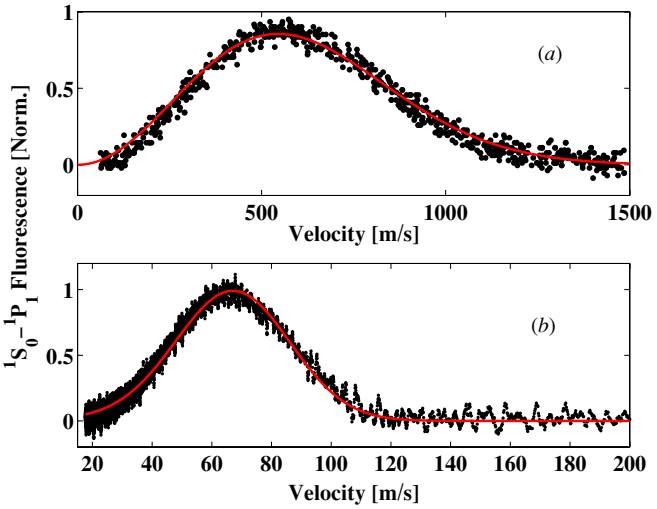

Figure 9. Velocity distributions from the oven (*a*) and after the deflection stage (*b*). (*a*) The velocity distribution is mapped by scanning the slowing laser frequency and observing the fluorescence from the beam (black). Shown with the red curve is the expected fluorescence signal for the atomic distribution from an oven operating at 456 °C. (*b*) The velocity distribution from the deflection stage is derived from a time-of-flight measurement on the atoms travelling from the deflection stage to the MOT chamber (black). The red curve is a fit to a Gaussian velocity distribution centred at 72 m s^{-1} and with a width of 26 m s^{-1}. Both theoretical curves in this figure take into account a $1/v$ weighting of the observed fluorescence.

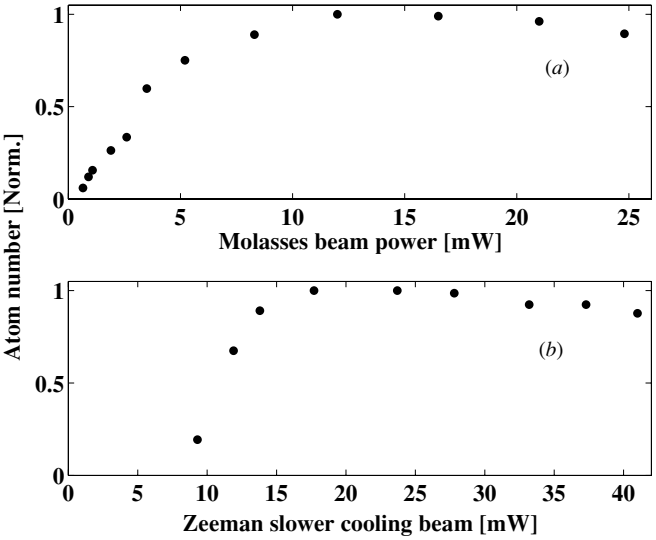

Figure 10. Variation of the MOT signal with power: (*a*) in the molasses beams of the deflection stage and (*b*) of the cooling laser beam of the Zeeman slower. The other parameters are: trap beams power 9 mW each; Zeeman slower main coil—9.5 A; end coil—2 A; Zeeman slowing laser beam at 26 mW and at a red detuning of 225 MHz; and Ca oven at 490 °C.

number of atoms is reached at a power of 12 mW. A further increase in the power leads to a gradual decrease in the number of trapped atoms. We associate this with increased heating in the 2D molasses resulting in a less collimated beam.

The relative number of trapped atoms is also investigated by varying the power in the slowing beam and the data are

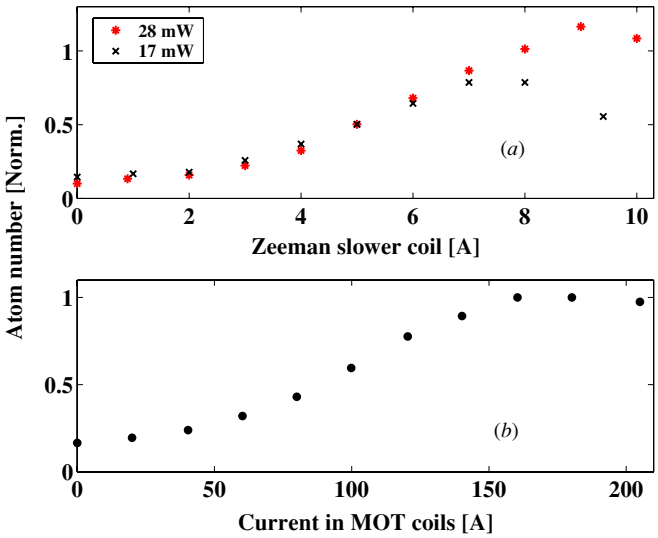

Figure 11. (*a*) MOT signal dependence on the main Zeeman slower coil current. The slowing laser beam is red detuned by 225 MHz and the end coil is near its optimum at 2A for all data points apart from the one at zero current, where it was also switched off. (*b*) MOT signal with the current in MOT coils for near optimum operating conditions of the Zeeman slower and deflection stage. The laser power in each MOT beam is 9 mW and the detuning is 23 MHz below resonance.

shown in figure 10(*b*). The optimum number is reached at about 18 mW. The slight decrease at higher powers is presumably due to increased transverse divergence of the beam and hence loss of atoms. The model shows good qualitative agreement with the threshold behaviour at low power but is inherently one dimensional so it does not include the effect of transverse heating.

The variation of the number of trapped atoms with the Zeeman slower coil current has been investigated for different slowing beam powers. Figure 11(*a*) shows that for currents up to about 5 A, the MOT slightly favours the lower power in agreement with the data shown in figure 10(*b*). However, at higher currents there is a significant reduction in the number of trapped atoms for the lower power. This has also been observed in our numerical model of the Zeeman slower. Higher coil currents result in steeper magnetic field gradients in the slower, and for the lower slowing beam power the scattering rate for atoms in the wings of the Gaussian light distribution is insufficient for them to stay on resonance. The optimum atom number appears not to depend strongly on the current in the end coil, which potentially could be left out in a future re-design of the set-up.

Also, shown in figure 11(*a*) is the number of trapped atoms in the MOT with the Zeeman slower coil switched off. From the ratio of trapped atoms with the slower off and on (maximum signal at 28 mW power), we see a factor of 12 increase in the MOT signal. Our Zeeman slower model indicates that in the absence of the field from the Zeeman slower, a narrow (typically less than 10 m s^{-1}) section of the initial velocity distribution around ∼200 m s^{-1} is slowed to the MOT capture velocity when the slowing laser beam is on. This represents less than 0.1% of the atoms. On the other hand, ∼19% of the atoms in the thermal distribution have velocities below 500 m s^{-1} for which the Zeeman slower is designed. Thus, we are clearly not capturing all the atoms in this range as this would have led to a more than 200-fold increase in the trapped atom number in going from zero to full current in the slower. We attribute this to the initial transverse velocity distribution of the atoms. The fraction of the thermal beam participating in the slowing process is defined by a solid angle determined by the slowing beam size and the interaction distance. In the experiment, this amounts to a half-angle of about 1° or less than half of what is defined by the oven capillaries. For an atom with an initial velocity of 200 m s^{-1} the corresponding transverse velocity is a few m s^{-1}, so after slowing to 70 m s^{-1} it still forms a reasonably collimated beam. However, atoms with an initial velocity of 500 m s^{-1} will have a transverse velocity distribution of order 10 m s^{-1}. This results in a more divergent slowed beam and a higher possibility of losing the atoms transversely before the two-dimensional cooling in the deflection stage. We attribute the less than expected increase in the MOT signal to this effective reduction in the acceptance angle of the slower for higher velocities.

The variation of the relative number of trapped atoms as a function of MOT coil current is shown in figure 11(*b*). As the current is increased, the field gradient steepens and the ability of the MOT to capture the atoms stopped in the light field increases. As the atoms enter the MOT region at an angle of 51° to the symmetry axis, they experience an effective field gradient reduced from the on-axis value of 32 G cm^{-1} to approximately 18 G cm^{-1}. The measured number of trapped atoms from the maximum of the MOT signal for the parameters shown in figure 11 is approximately 10^6.

3.1. Lifetime of the trap

In addition to optimizing the apparatus as described above, we carried out measurements of the storage time of the atoms in the trap. As the intensity is increased in the MOT beams, the scattering rate on the cooling transition increases as does the loss out of the cooling cycle through decay to the $^1D_2$ state and on to the $^3P_2$ state. Thus, the optimum MOT power is a compromise between, on the one hand, having sufficient intensity to efficiently capture the atoms and, on the other, low enough intensity to achieve a reasonable lifetime.

The lifetime of the calcium atoms in the magneto-optical trap depends on a number of experimental parameters including background collisions, inelastic two-body collisions between cold atoms and losses due to the atomic level structure through spontaneous decay to levels not participating in the cooling cycle. For typical experimental conditions, the latter is the dominant and has already been studied in the literature [16, 32–34].

For the measurement of the lifetime of the Ca MOT, we used a mechanical chopper at the deflection/molasses stage laser beam. The loading (decay) curves are taken for different on (off) times of the deflection beams at different intensities of the MOT beams. All the measurements are taken for a fixed detuning of the MOT beams. From the single exponential fit to the data, the trap lifetimes are extracted. The measured values are shown in figure 12 and are in good agreement with

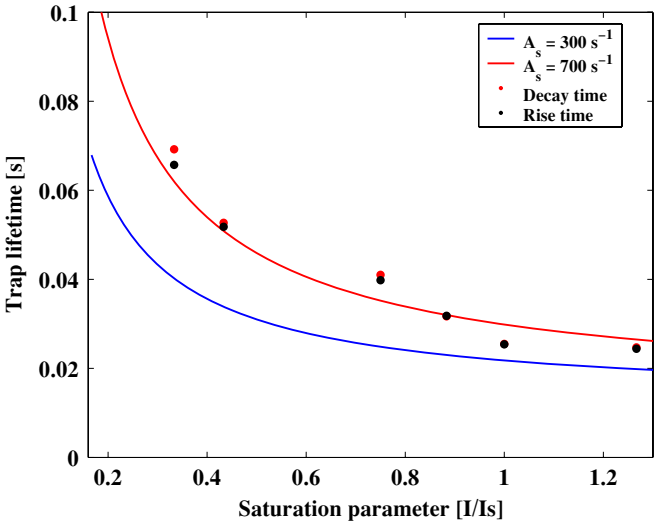

Figure 12. Variation of the lifetime of the trapped atoms with the total intensity in the MOT beams. The fluorescence of the MOT was recorded while the atomic beam was modulated (on/off). The time constants for the corresponding filling and decay of the MOT are shown as black and red points, respectively. The statistical error on these measurements is estimated at 2%. The curves shown in blue ($A_s = 300\ \mathrm{s}^{-1}$) and red ($A_s = 700\ \mathrm{s}^{-1}$) are calculated using a rate equation model for the levels participating in the cooling cycle. See the text for details.

experimental values reported in the literature [16, 33, 34]. It shows the expected decrease in lifetime with increasing laser intensity of the trap laser beams.

To estimate the parameters that influence the lifetime of the trap, we have solved the rate equations for a four-level system under steady-state conditions. Taken into account are the $^1S_0$,$^1P_1$,$^1D_2$ and $^3P_2$ states only, assuming that atoms decaying to the $^3P_1$ state (a lifetime of 0.4 ms) rejoin the cooling cycle. The $^3P_2$ state atoms are treated as a loss from the system. Using the nomenclature from [33] the expression for the lifetime (τ) of the MOT after solving the rate equations for the four-level system simplifies to

$$\tau = \left(1 + \frac{A_\mathrm{P} + A_\mathrm{S}}{A_\mathrm{P-D}} \frac{1}{f}\right) \frac{1}{A_\mathrm{P} + \epsilon A_\mathrm{S}}, \qquad (3)$$

where, $A_\mathrm{P-D}$ is the decay rate on the $^1P_1$–$^1D_2$ transition, A_P is the decay rate on the $^1D_2$–$^3P_2$ transition and A_S is the mean spontaneous decay from the $^1D_2$ state to the ground state via the $^3P_1$ state. ϵ is the fraction of atoms that are sufficiently fast to escape the trap before decaying from the $^1D_2$ state. The excitation rate, f, is defined as

$$f = \frac{1}{2} \frac{\frac{I}{I_s}}{1 + \frac{I}{I_s} + \left(\frac{2\Delta}{\Gamma}\right)^2}, \qquad (4)$$

where Δ is the detuning of the trap laser beams, Γ is the decay rate of the $^1P_1$ state, I_s is the saturation intensity and I is the intensity of the trap laser beams.

The expression equation (3) differs slightly from the one that appears in the literature [32]. The difference is the term represented by factor 1 in the bracket. This term comes from the full four-level rate equation analysis of the problem and represents $^1D_2$ atoms that take part in the cooling cycle. The effect of it is to increase the calculated trap lifetime by approximately 10 ms. This partly resolves the discrepancy observed in previous MOT lifetime measurements [33]. Disregarding this term is equivalent to assuming negligible population in the $^1D_2$ state. However, for our typical operating conditions the steady-state population in the $^1D_2$ state is approximately 57% of the trapped atoms.

Parameter ϵ needs to be estimated for the particular experimental conditions. Doppler cooling will result in a velocity spread of approximately 1.5 m s^{-1}. For the purpose of this estimate, we assume a $^1D_2$ lifetime of 1.5 ms and that atoms that move more than 10 mm before they return to the ground state are lost from the cooling cycle. This results in $\epsilon = 4.2\%$ for our typical experimental conditions.

The decay rates appearing in equation (3) are all rather small and correspondingly hard to measure. Values of $A_\mathrm{P-D} = 2180(300)\ \mathrm{s}^{-1}$, $A_\mathrm{P} = 96(20)\ \mathrm{s}^{-1}$ and $A_\mathrm{S} = 300(90)\ \mathrm{s}^{-1}$ have been used regularly in the literature [18, 32, 33]. However, $^1D_2$ lifetimes varying from 1.5 to 2 ms [19, 35] have been reported in disagreement with these decay rates.

The curve shown in blue in figure 12 is calculated based on $A_\mathrm{S} = 300\ \mathrm{s}^{-1}$. It yields a lifetime 10–20% shorter than the measured values at the higher intensities increasing to twice that at lower intensities. A similar discrepancy is apparent in the data published by the PTB group [33] after inclusion of the additional term from equation (3). However, if we assume a larger decay rate from the $^1D_2$ state commensurate with the observations of a shorter lifetimes, the agreement is better. The curve obtained for $A_\mathrm{S} = 700\ \mathrm{s}^{-1}$ is shown in red (figure 12). The agreement with the measured lifetime data indicates a $^1D_2$ lifetime in the region of 1.25 ms. The value of $A_\mathrm{P} = 96\ \mathrm{s}^{-1}$ has been maintained for this curve. However, there is no reason to suspect that this number is any more accurate than the reported A_S values, but we do not have data over a sufficient intensity range to fit two parameters. Equation (3) does, however, indicate different dependencies of the MOT lifetime on A_S and A_P, so a range of carefully conducted measurements could yield accurate values for both parameters and thereby provide valuable insight into the dominant loss mechanism for a Ca MOT.

To increase the lifetime of the MOT as well as the atom number, we have used a second (repump) laser at 672 nm to drive atoms from the singlet $^1D_2$ state to the higher 4s5p $^1P_1$ state. While the branching ratio to the ground state from this high level is only 1 : 44 [36], the transition is strong enough that the additional laser rapidly pumps the $^1D_2$ atoms to the ground state. Our preliminary measurements show a factor of 5 increase in the lifetime of the trap as well as the atom number.

A number of techniques have been used for cold atom temperature measurements, but the relatively large steady-state population of Ca atoms in the $^1D_2$ state may also affect such measurements. One-dimensional Doppler cooling theory yields an expected value of 1.7 mK for the detuning and intensity applied for the present experiment [4]. Using a three-dimensional model of the MOT for (1+3)-level atoms it is suggested that the presence of coherences between the magnetic sublevels in the excited state may increase the

temperature depending on the light intensity and detuning of the trap beams [37]. At this temperature, the Ca MOT lends itself to implementation of the release and recapture method [31, 38]. With this technique the MOT laser beams are extinguished for a brief period of time allowing the atoms to expand ballistically before the light comes back on again and recaptures any atoms that are still within the capture volume. For a capture volume of order 1 cm^3 and an rms velocity of order 1.5 m s^{-1} ballistic expansion times up to 10 ms are required to yield an estimate for the temperature. However, during this time the $^1D_2$ atoms decay spontaneously providing a significant increase in the ground-state population partly obscuring the loss of atoms due to ballistic expansion.

Similarly, temperature determinations based on the size of the MOT and knowledge of the magnetic field gradient are affected by the sizable $^1D_2$ population. Normally this measurement is done by equating the atomic kinetic energy with the inferred potential energy of the MOT based on the observed size. However, this does not take into account that while the atoms occupy the $^1D_2$ state they expand virtually unaffected by the MOT. They will return to the ground state and start scattering light again at a distance from the centre, somewhat larger than that expected from the temperature and field gradient. The most reliable technique for measuring the temperature of a Ca MOT would appear to be the direct mapping of the Doppler broadened shape of the $^1S_0$–$^3P_1$ intercombination line at 657 nm [8, 33].

4. Summary

We have reported in detail a compact (total length less than 800 mm) apparatus for laser cooling and magneto-optical trapping of calcium atoms. The compactness of the set-up arises mainly from the Zeeman slower section that has an over all length of 140 mm compared to all the existing calcium set-ups. A shorter Zeeman slower reduces the loss of atoms due to the transverse spreading of the beam as well as reduces the laser power requirement. The deflection stage has the advantage of isotope selective trapping of atoms. We make use of the strong $^1S_0$–$^1P_1$ 423 nm transition for trapping the calcium atoms in the ground state. The design and operation of the various sections of the apparatus including the optical set-up, the Ca oven, the Zeeman slower, the deflection/transverse molasses stage and MOT are described. The optimization of these stages is done by monitoring the fluorescence signal from trapped atoms. The MOT lifetime is measured for a range of laser intensities and compared with a rate equation model. This more complete description, to be presented elsewhere [21], reveals an additional contribution to the MOT lifetime, which has previously been disregarded. It also demonstrates that accurate MOT lifetime measurements could provide valuable information to resolve discrepancies in the $^1D_2$ decay rates reported in the literature. The trap lifetime and the atom number can be further increased using repump lasers at 672 nm and 1530.5 nm. Details of this will be reported elsewhere [21]. The 1530.5 nm laser drives the $^1D_2$–$^3P_2$ transition, which is the only leak channel, and thus makes it a closed cooling system. It also provides access to the 'lost' atoms in the $^3P_2$ state that are magnetically trapped in the quadrupole field from the MOT coils. Cold and trapped Ca atoms can then be used for further studies to explore the feasibility of achieving Bose–Einstein condensation in an alkaline earth element.

Acknowledgments

This work was supported by the UK Engineering and Physical Sciences Research Council (EPSRC). MB acknowledges support from the European Union ERASMUS exchange student programme. We acknowledge Aidan Arnold and Paul Griffin for careful reading of the manuscript.

References

[1] Raab E L, Prentiss M, Cable A, Chu S and Pritchard D E 1987 Trapping of neutral sodium atoms with radiation pressure *Phys. Rev. Lett.* **59** 2631–4
[2] Anderson M H, Ensher J, Mathews M, Weiman C and Cornell E 1995 Observation of Bose–Einstein condensation in a dilute atomic vapor *Science* **269** 198–201
[3] Davis K B, Mewes M, Andrews M, Van Druten N, Durfee N, Kurn D and Ketterle W 1995 Bose–Einstein condensation in a gas of sodium atoms *Phys. Rev. Lett.* **75** 3969–73
[4] Adams C S and Riis E 1997 Laser cooling and trapping of neutral atoms *Prog. Quantum Electron.* **21** 1
[5] Pereira Dos Santos F, Leonard J, Wang J, Barrelet C J, Perales F, Rasel E, Unnikrishnan C S, Leduc M and Cohen-Tannoudji C 2001 Bose–Einstein condensation of metastable helium *Phys. Rev. Lett.* **86** 3459–62
[6] Robert A, Browaeys O, Poupard J, Nowak S, Boiron D, Westbrook C I and Aspect A 2001 A Bose–Einstein condensate of metastable atoms *Science* **292** 461–4
[7] Takasu Y, Maki K, Komori K, Takano T, Honda K, Kumakura M, Yabuzaki T and Takahashi Y 2003 Spin-singlet Bose–Einstein condensation of two-electron atoms *Phys. Rev. Lett.* **91** 040404
[8] Oates C W, Bondu F, Fox R W and Hollberg L 1999 A diode-laser optical frequency standard based on laser-cooled Ca atoms: sub-kilohertz spectroscopy by optical shelving detection *Eur. Phys. J.* D **7** 449–60
[9] Campbell G K *et al* 2008 The absolute frequency of the ^{87}Sr optical clock transition *Metrologia* **45** 539–48
[10] Hansen D and Hemmerich A 2006 Observation of multi-channel collisions of cold metastable calcium atoms *Phys. Rev. Lett.* **96** 073003
[11] Keupp J, Douillet A, Mehlstaubler T E, Rehbein N, Rasel E M and Ertmer W 2005 A high-resolution Ramsey–Bordé spectrometer for optical clocks based on cold Mg atoms *Eur. Phys. J.* D **36** 289
[12] Ido T, Isoya Y and Katori H 2000 Optical-dipole trapping of Sr atoms at a high phase-space density *Phys. Rev.* A **61** 061403
[13] Xu X, Loftus T H, Dunn J W, Greene C H, Hall J L, Gallagher A and Ye J 2003 Single-stage sub-Doppler cooling of alkaline earth atoms *Phys. Rev. Lett.* **90** 193002
[14] Daley A J, Boyd M M, Ye J and Zoller P 2008 Quantum computing with alkaline-earth-metal atoms *Phys. Rev. Lett.* **101** 170504
[15] Boyd M M, Zelevinsky T, Ludlow A D, Blatt S, Zanon-Willette T, Foreman S M and Ye J 2007 Nuclear spin effects in optical lattice clocks *Phys. Rev.* A **76** 022510
[16] Hoekstra S, Mollema A K, Morgenstern R, Wilschut H W and Hoekstra R 2005 Single-atom detection of calcium isotopes by atom-trap trace analysis *Phys. Rev.* A **71** 023409
[17] Sansonetti J E and Martin W C 2005 Handbook of basic atomic spectroscopic data *J. Phys. Chem. Ref. Data* **34** 1559

[18] Beverini N, Giammanco F, Maccioni E, Strumia F and Vissani G 1989 Measurement of the calcium $^1P_1$–$^1D_2$ transition rate in a laser-cooled atomic beam *J. Opt. Soc. Am.* B **6** 2188–93
[19] Drozdowski R, Kwela J and Walkiewicz M 1993 Lifetimes of the 4s4p $^3P_1$ and 4s3d states in Ca I *Z. Phys.* D **27** 321–4
[20] Grünert J and Hemmerich A 2001 Optimizing the production of metastable calcium atoms in a magneto-optical trap *Appl. Phys.* B **73** 815–18
[21] Dammalapati U, Norris I and Riis E 2009 Saturated absorption spectroscopy of calcium in a hollow cathode lamp *J. Phys. B: At. Mol. Opt. Phys.* **42** at press
[22] Grünert J and Hemmerich A 2002 Sub-Doppler magneto-optical trap for calcium *Phys. Rev.* A **65** 041401
[23] Torabi-Goudarzi F and Riis E 2003 Efficient CW high-power frequency doubling in periodically poled KTP *Opt. Commun.* **227** 389–403
[24] Dammalapati U, Norris I and Riis E 2009 Laser spectroscopy of the 4s3d $^1D_2$ and 4s4p $^3P_2$ states cold calcium atoms (in preparation)
[25] Murray A J, Hussey M J and Needham M 2006 Design and characterization of an atomic beam source with narrow angular divergence for alkali-earth targets *Meas. Sci. Technol.* **17** 3094–101
[26] Ramsey N F 1956 *Molecular Beams* (Oxford: Clarendon)
[27] Phillips W D and Metcalf H 1982 Laser deceleration of an atomic beam *Phys. Rev. Lett.* **48** 596–9
[28] De S, Dammalapati U, Jungmann K and Willmann L 2009 Magento-optical trapping of barium *Phys. Rev.* A **79** 041402
[29] Adams C S, Arnold A, Cox S G and Riis E 2003 Laser cooling of calcium in a 'golden ratio' quasi-electrostatic lattice *J. Phys. B: At. Mol. Opt. Phys.* **36** 1933–42
[30] Weatherill K J, Pritchard J D, Griffin P F, Dammalapati U, Adams C S and Riis E 2009 A versatile and reliably reusable ultrahigh vacuum viewport *Rev. Sci. Instrum.* **80** 026105
[31] Lett P D, Watts R N, Westbrook C I and Phillips W D 1988 Observation of atoms laser cooled below the Doppler limit *Phys. Rev. Lett.* **61** 169–72
[32] Kurosu T and Shimizu F 1992 Laser cooling and trapping of alkaline earth atoms *Japan. J. Appl. Phys.* **31** 908–12
[33] Kisters Th, Zeiske K, Reihle F and Helmcke J 1994 High-resolution spectroscopy with laser-cooled and trapped calcium atoms *Appl. Phys.* B **59** 89–98
[34] Grünert J, Quehl G, Elman V and Hemmerich A 2000 Ultracold metastable calcium ensembles, a medium for matter wave amplification? *J. Mod. Opt.* **47** 2733–40
[35] Daily J E, Gommers R, Cummings E A, Durfee D S and Bergeson S D 2005 Two-photon photoionization of the Ca 4s3d $^1D_2$ level in an optical dipole trap *Phys. Rev.* A **71** 043406
[36] Ralchenko Yu, Kramida A E and Reader J (NIST ASD team) 2008 *NIST Atomic Spectra Database*
[37] Choi S K, Park S E, Chen J and Minogin V G 2008 Three-dimensional analysis of the magneto-optical trap for (1+3)-level atoms *Phys. Rev.* A **77** 015405
[38] Mollema A K 2008 Laser cooling, trapping and spectroscopy of calcium isotopes *PhD Thesis* University of Groningen, The Netherlands